



City Research Online

City, University of London Institutional Repository

Citation: Khaled, A., Hameed, M. F. O., Rahman, B. M. ORCID: 0000-0001-6384-0961, Grattan, K. T. V. ORCID: 0000-0003-2250-3832, Obayya, S. S. A. and Hussein, M. (2020). Characteristics of silicon nanowire solar cells with a crescent nanohole. *Optics Express*, 28(21), pp. 31020-31033. doi: 10.1364/OE.397051

This is the published version of the paper.

This version of the publication may differ from the final published version.

Permanent repository link: <https://openaccess.city.ac.uk/id/eprint/25698/>

Link to published version: <http://dx.doi.org/10.1364/OE.397051>

Copyright and reuse: City Research Online aims to make research outputs of City, University of London available to a wider audience. Copyright and Moral Rights remain with the author(s) and/or copyright holders. URLs from City Research Online may be freely distributed and linked to.

City Research Online:

<http://openaccess.city.ac.uk/>

publications@city.ac.uk



Characteristics of silicon nanowire solar cells with a crescent nanohole

AWAD KHALED,¹ MOHAMED FARHAT O. HAMEED,^{1,2,3}  B. M. A. RAHMAN,⁴ K. T. V. GRATTAN,⁴ S. S. A. OBAYYA,^{1,*}  AND MOHAMED HUSSEIN^{1,5}

¹Centre for Photonics and Smart Materials, Zewail City of Science and Technology, October Gardens, 6th of October City, Giza 12578, Egypt

²Nanotechnology and Nanoelectronics Engineering Program, Zewail City of Science and Technology, October Gardens, 6th of October City, Giza 12578, Egypt

³Mathematics and Engineering Physics Department, Faculty of Engineering, Mansoura University, Mansoura 35516, Egypt

⁴Department of Electrical and Electronic Engineering, City, University of London, London EC 1 V 0HB, United Kingdom

⁵Physics Department, Faculty of Science, Ain Shams University, Cairo, Egypt

*sobayya@zewailcity.edu.eg

Abstract: In recent years, newly emerging photovoltaic (PV) devices based on silicon nanowire solar cells (SiNW-SCs) have attracted considerable research attention. This is due to their efficient light-trapping capability and large carrier transportation and collection with compact size. However, there is a strong desire to find effective strategies to provide high and wideband optical absorption. In this paper, a modified circular nanowire (NW) with a nanocrescent hole is newly introduced and analyzed for solar cell applications. The crescent hole can strongly improve the light absorption through the NW due to the excitation of numbers of modes that can be coupled with the incident light. The material index, volume, and position of the nanohole are studied to significantly increase the optical absorption efficiency and hence the power conversion efficiency (PCE). The absorption performance can be further preserved by using a silicon substrate due to the coupling between the supported modes by the NW, and that of the substrate. The optical and electrical characteristics of the suggested design are investigated using finite difference time domain and finite element methods via Lumerical software packages. The reported asymmetric design offers higher optical and electrical efficiencies compared to the conventional NW counterpart. The proposed NW offers a short circuit current density (J_{sc}) of 33.85 (34.35) mA/cm² and power conversion efficiency (PCE) of 16.78 (17.05) % with an enhancement of 16.3 (16.8) % and 17.3 (18.4) % for transverse magnetic (TM) and transverse electric (TE) polarizations, respectively, compared to the conventional cylindrical counterpart.

© 2020 Optical Society of America under the terms of the [OSA Open Access Publishing Agreement](#)

1. Introduction

Nowadays, there is a rapid increase in using renewable energy resources in our daily life. A transition from fossil fuel-based energy to sustainable and clean energy resources plays an important role in this aspect. It is highly aimed, in the photovoltaic (PV) community, to reduce the amount of used silicon (Si) in solar cells (SC) to decrease its overall cost. This can be achieved by using thin film (TF) SC with a thickness of few micrometers [1–4]. Further, the thinner Si wafers have several advantages such as realization of efficient carrier diffusion and collection under a short transport length. Additionally, lower-quality materials can be used for PV products at a low cost. However, thin c-Si wafers have low optical absorption due to its indirect-bandgap [5].

In order to boost the absorbed light and power conversion efficiencies of the TFSC, several strategies based on nanotechnologies have been employed. In this regard, nanopillars [6],

nanowires [7,8], nanocones [9–11], nanoholes [12–14], nanodomes [15], nanostars [16], nanopyramids [17–20], and nanopencils [21,22], have been used at the front and/or back side of the absorber layer to reflect, diffract, and refract light, to increase the total optical path length within the cell [23–26]. Previous studies showed that controlling the size, geometry and orientation of the nanowire (NW) can readily tune the light absorption within the NW [8,27]. In this regard, several designs have been introduced, analyzed and fabricated such as cylindrical, rectangular, conical, stars and funnels NWs. Further, Hussein *et al.*, have proposed funnel shaped SiNWs with an efficiency as high as 41.8% [28] and PCE of 14.13% [29]. Furthermore, it has been shown that the NWs distributed in a rectangular geometry have higher external quantum efficiency (EQE) than the hexagonal arrangement with the same volume [30,31]. Korany *et al.*, [32] have studied the optical and electrical characteristics of the conical structures with an optical efficiency of 44.21% and electrical efficiency of 17.21%.

Moreover, other studies have reported improved performance of the SCs based on different materials such as indium phosphide [33,34], gallium arsenide [35,36], zinc oxide [37,38], crystalline silicon [39–42], amorphous silicon alloys [43–45]. It has been reported that different positions [46] and nano-hole (NH) diameters combinations [47] can improve the optical absorption efficiency of centered nano-hole arrays. Perpendicular elliptical nanohole arrays break the symmetry of circular arrays, thus boosting the number of modes that can be coupled with the incident light [48]. Changing the rotation angle of the elliptical NH properly around its axis to adjust the distance between the adjacent NH wall can also significantly increase optical absorption efficiency. These results indicate that an asymmetrical design has better optical absorption than symmetric counterparts. Further, Zhang *et al.*, [49] showed that SiNWs with an asymmetrical nanovoid design can improve the short circuit current density by 37.5% over the conventional solid nanowire devices with reduced photoactive material. Further, Yang *et al.*, [46] reported that the broken angular symmetry of the NW could improve the light-harvesting performance with photocurrent density enhancement of 45% over the conventional counterpart. In this paper, we introduce a NWSC with a crescent nanohole to improve the absorption in most of the visible and ultraviolet bands.

In this study, the optical and electrical parameters of the proposed design are studied by using the finite difference time domain (FDTD) and finite element (FEM) methods and compare the performance parameters with conventional solid NW counterparts. It is worth mentioning that by controlling the material index, volume, and position of the nanohole the absorption efficiency can be maximized and hence the power conversion efficiency (PCE). The proposed design achieves considerable light absorption improvement due to the excitation of reinforced resonances of the nanohole cavity. The suggested NW with crescent NH shows an optical absorption enhancement of 22.5% and (12.89%) for TM and (TE) polarizations, respectively, compared to the conventional solid NWs counterparts. Additionally, the PCE is also improved by 17.3% (18.4%) relative to the conventional solid NWs. Further, the suggested design has better PCE than funnel shaped NW [29], by 18.75% and is comparable to conical NWs reported in [32].

2. Simulation strategy

2.1. Optical simulation

Figure 1(a) displays a schematic diagram of the proposed SiNW SC with a crescent nano hole. The modified SiNW has a radius R while the crescent nanohole has an inner and outer radii of r_i and r_o , respectively, as revealed from Fig. 1(a). The crescent nanohole is shifted from the NW center by distances d_x , and d_y in the x and y directions, respectively. In this study, the structure periodicity Λ , nano wire height h , crescent nanohole depth v , and radius R are initially taken as 500 nm, 2330 nm, 2330 nm and 200 nm, respectively. To evaluate the absorption spectra of the suggested SiNWs under plane wave incidence, 3D finite difference time domain (FDTD) is used via Lumerical software package [50]. The periodic boundary conditions are employed in x - and

y-directions to create an infinite periodic square array. However, a perfectly matched layer (PML) boundary condition is also used along the top and bottom boundaries in z-direction as shown in Fig. 1(a) to absorb any radiated modes and reduce unnecessary reflections. The absorption $A(\lambda)$ is defined as the fraction of the absorbed incident light in the NWs at wavelength λ , which can be calculated from the transmission $T(\lambda)$ and reflection $R(\lambda)$ as follows

$$A(\lambda) = 1 - T(\lambda) - R(\lambda). \quad (1)$$

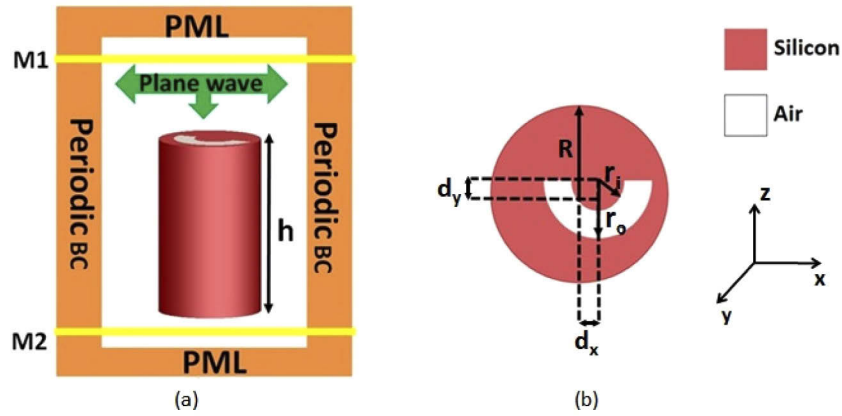


Fig. 1. (a) The simulated 3D computational domain of the modified Si NW unit cell, and (b) cross-section of the suggested Si NW in x-y plane.

In order to calculate the $T(\lambda)$ and $R(\lambda)$, two monitors are placed below and above the studied NW as shown in Fig. 1(a). In this investigation, the refractive index of the Si is taken from Palick model reported in [51]. To evaluate the absorption capabilities of the proposed SiNWs with a crescent nano hole, the ultimate efficiency η , is calculated as follows:

$$\eta = \frac{\int_{300}^{\lambda_g} F_s(\lambda) \frac{\lambda}{\lambda_g} A(\lambda) d\lambda}{\int_{300}^{4000} F_s(\lambda) d\lambda}. \quad (2)$$

Where λ_g is the Si bandgap wavelength, and $F_s(\lambda)$ is the photon flux density in the AM 1.5 solar spectral irradiance. In this study, λ_g is taken as 1100 nm; corresponding to the silicon material energy gap. Additionally, based on charge of electron e , plank's constant h and , the short circuit current density J_{sc} is calculated as follows:

$$J_{sc} = \eta \frac{e \lambda_g}{hc} \cdot \int_{300nm}^{4000nm} F_s(\lambda) d\lambda = 81.83 \times \eta (\text{mA/cm}^2). \quad (3)$$

2.2. Electrical simulation

From a practical point of view, it is necessary to perform an electrical stimulation for the studied design. This is a vital step for the design of the solar cells , because the J_{sc} is overestimated in a pure optical design that assumes a perfect internal quantum efficiency (i.e., IQE=100%). In the optical analysis, all carrier loss mechanisms are neglected during carrier transportation and recombination. Further, it is previously assumed that every photon with greater than the silicon bandgap produces one and only one electron hole pair. The electrical characterization of the suggested design is carried out further by using the 3D finite element method via the Lumerical Software package. Figures 2(a) and 2(b) show the schematic diagrams of a square array of the crescent NWs and a unit cell with an axial (p-i-n) doping fixed on Si-substrate, while

the top contact of the crescent NWs is used as an emitter. Additionally, the substrate entire area is enveloped with bottom contact which is used as a base as shown in Fig. 2. The crescent NWSC geometrical parameters are listed in Table 1.

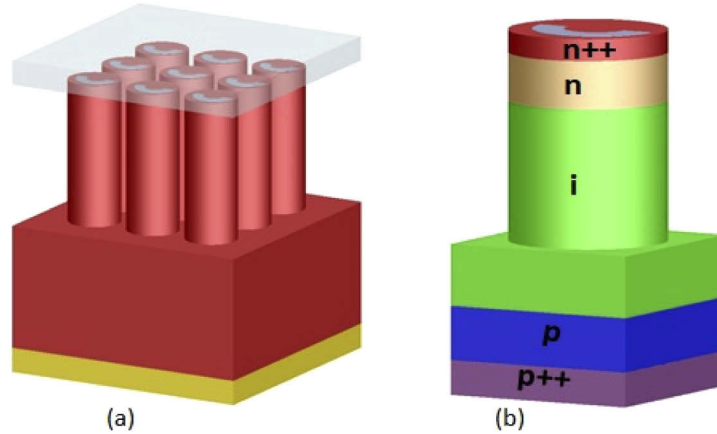


Fig. 2. Schematic diagram of (a) the vertically aligned crescent NWs array and (b) the axial p-i-n junction of the proposed NW.

Table 1. The geometrical parameters of the suggested NWSC.

Parameter	Description	Nominal value
R	Nanowire radius	200 nm
r_i	crescent nanohole inner radius	80 nm
r_o	crescent nanohole outer radius	160 nm
v	crescent nanohole depth	2330 nm
d_x	sidelong deviation distance	15 nm
d_y	deviance distance	15 nm
h	Nanowire height	2330 nm

Table 2. The geometrical parameters of the doping concentrations.

Doping layer	n++	n	i	p	P++
Thickness (nm)	50	250	3350	400	80

3. Results and discussion

3.1. Optical results

Figures 3(a) and 3(b) show the simulated absorption spectra for both conventional solid cylindrical SiNWs and the proposed SiNWs with the crescent nanohole for transverse electric (TE) and transverse magnetic (TM) polarizations. In this study, the geometrical parameters values are $R = 200$ nm, $r_i = 80$ nm, $r_o = 160$ nm, $d_x = 15$ nm and $d_y = 15$ nm, as shown in Table 2. It is evident from Fig. 3 that the proposed design offers better absorption efficiency in short and long wavelengths than conventional cylindrical solid NWs for TE and TM polarizations. The conventional cylindrical NWs array cannot support some modes owing to its mirror symmetry

[52,53]. The point group symmetry of the unit cell of a circular NW array contains a four-fold rotation axis and four mirror planes. Therefore, the use of asymmetric crescent nanohole through the NW will remove the mirror symmetry of the proposed NW. Therefore, the number of bands that can be coupled with external incident light will be increased with absorption enhancement. Further, vertical channeling modes are supported in the crescent nanohole, which is favorable to the absorption of incident light. This is due to the enhancement in antireflection caused by the channeling modes concentration in the low-index crescent nanoholes [54]. To understand the absorption enhancement through the crescent nanohole NW, the electric field distributions in the x - y plane are shown in Figs. 3(c) and 3(e) for TE and TM polarizations at wavelength of 496 nm. Additionally, the field distribution through the solid NW is depicted in Figs. 3(d) and 3(f). It may be seen from these figures that the resonant modes are more complex in the NW with the crescent nanohole than the solid NW. This is owing to the nanohole defect inside the NW which adjusts the interior resonant nature dramatically and produces stronger resonances. Therefore, the absorption and hence the J_{sc} are improved as shown in Figs. 3(a) and 3(b), and listed in Table 3.

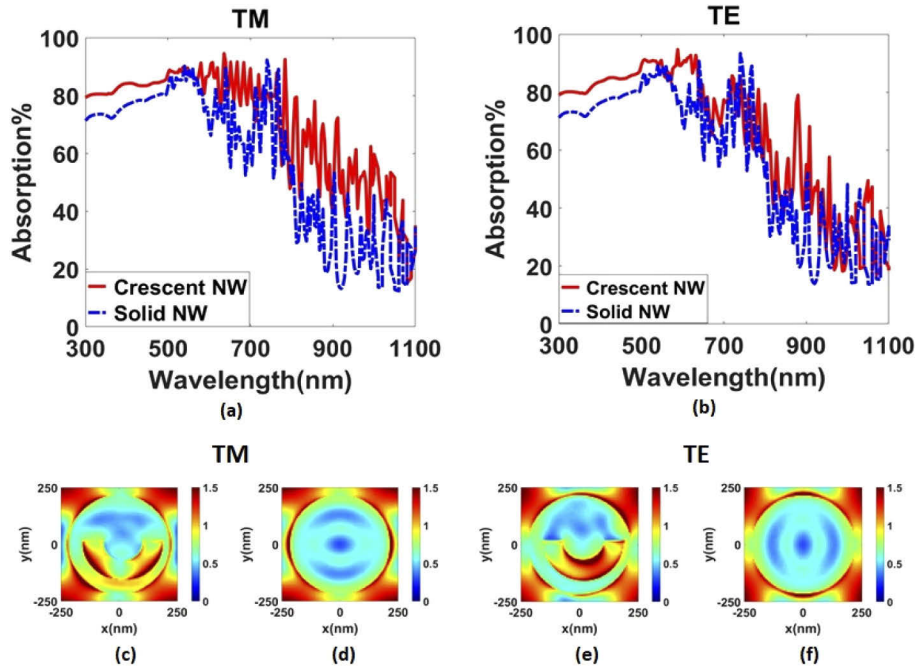


Fig. 3. Absorption of the modified Si NW and solid SiNW at $R=200$ nm for (a) TM and (b) TE polarizations. The electric field profiles in the x - y plane are shown through the (c,e) suggested crescent Si NW and (d,f) solid Si NW at $\lambda = 496$ nm, and $R = 200$ nm, $r_1 = 80$ nm, $r_0 = 160$ nm, $d_x = 15$ nm and $d_y = 15$ nm.

Table 3. The ultimate efficiency and short circuit current density of the suggested design and the solid NW.

Parameters	Proposed NW		Solid NW	
	TE	TM	TE	TM
η %	32.4	34.8	28.7	28.4
J_{sc} (mA/cm ²)	26.5	28.5	23.4	23.2

To further emphasize the implied mechanism of the absorption improvement, the field profiles through the solid NW is studied. Figure 4 shows the steady-state field profiles in the x - z plane for the suggested crescent nanowire and the conventional solid cylindrical at $\lambda = 924$ nm for TE and TM polarizations. It is evident that more incident light is coupled with the supported modes through the suggested crescent nanowire arrays than the conventional NW. The coupled light has been absorbed by the active material which enhances the electron hole pair generation and power conversion efficiency through the suggested NW. This is compatible with that reported in [55] with off-axial core/shell silicon NWs where the photoactive region is deviated from the shell center. It has been shown that the asymmetric core/shell design has a dramatic improved light absorption over a broadband of wavelengths. Such an absorption enhancement is mainly due to the strengthened nanofocusing effect with improved coupling between the photoactive material and the focus of the dielectric shell [55].

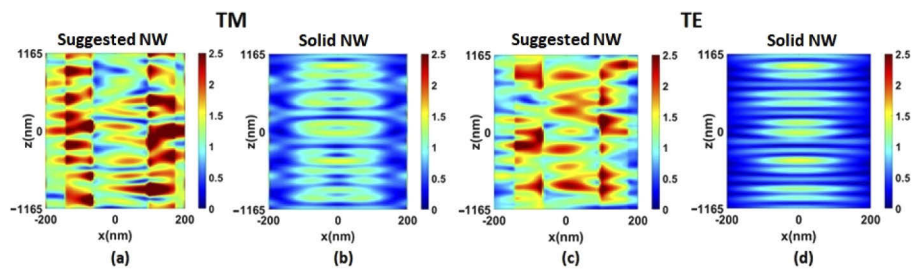


Fig. 4. Absorption field profiles in x - z plane at $\lambda = 924$ nm for (a, b) TM, and (c, d) TE polarizations.

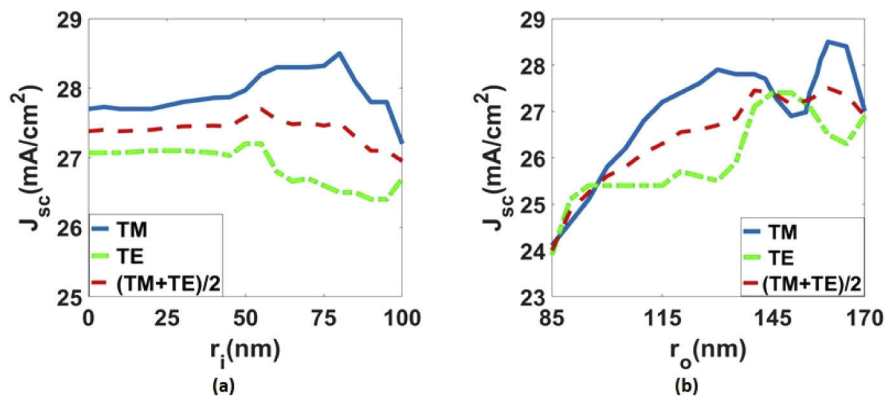


Fig. 5. Short-circuit current density versus (a) the inner radius r_i , and (b) the nanohole outer radius r_o .

The geometrical parameters are studied thoroughly to improve the light absorption and minimize the reflection. First, the effect of shifting the center of the crescent nanohole layer upwards or downwards from the central position as shown in the inset of Fig. 5. Figure 5(a) shows the variation of the J_{sc} with the deviance distance d_y from the center while the other parameters are kept constants at their initial values. It can be seen that as d_y is increased from 0 to 15 nm, the J_{sc} is increased to maximum value of 28.5 mA/cm². Figure 5(c) shows the norm component of the fundamental TM mode through the suggested NW at $d_x = d_y = 15$ nm. It may be seen that the fundamental mode is well confined through the NW which can produce high absorption through the active layer. If d_y is further increased to 70 nm, the outward leakage of

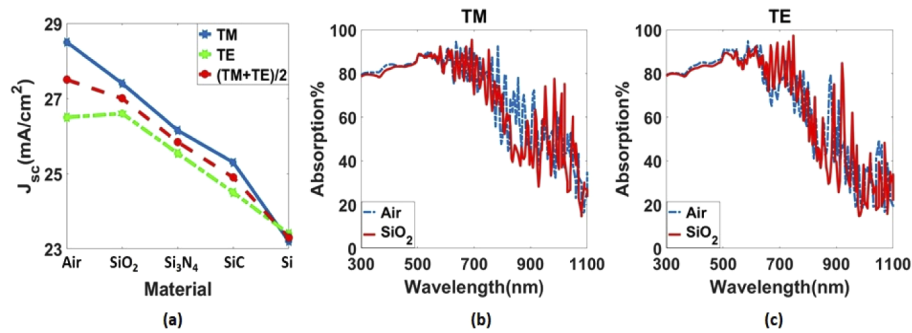


Fig. 6. (a) J_{sc} versus the refractive index n of the filling materials. The absorption spectra of the NWSCs with nanoholes filling with air and SiO₂ under (b) TM and (c) TE incidences, respectively.

the fundamental mode will be increased with increased radiation losses as shown in Fig. 5(d). This will reduce the absorption and hence the J_{sc} to 25.4 mA/cm². Therefore, $d_y = 15$ nm will be used in the subsequent simulations. Next, the impact of the sidelong deviation d_x of the nanohole on the NW solar absorption is studied. Figure 5(b) illustrates the short circuit current density J_{sc} dependence on the sidelong deviation d_x under TM, TE, and unpolarized cases. It may be seen that the J_{sc} curve is symmetric around $d_x = 0$ nm and $d_y = 15$ nm for the studied polarizations. Further, maximum J_{sc} of 28.5 mA/cm² can be obtained for TM polarization with an improvement of 22.8% at $d_x = 15$ nm. If d_x is further increased to 40 nm, the leakage of the fundamental mode and hence the radiation losses will be increased as shown in Fig. 5(e). This will reduce the absorption and hence the J_{sc} to 27.01 mA/cm². Notably, the position of the crescent nanohole inside the NW is critical, which should be configured in an asymmetrical way to improve optical absorption. The geometrical parameters of the other design are tuned to further improve the optical efficiency of the reported design. Figure 6(a) shows the relation between J_{sc} and r_i while the other parameters are fixed at $d_y = 15$, $d_x = 15$, $R = 200$, $r_o = 160$ nm. It can be noted that as r_i increases, the J_{sc} is also increased. The maximum J_{sc} is attained at $r_i = 80$ nm. Figure 6(b) shows the variation of the J_{sc} with the nanohole radius r_o while the other parameters d_y , R , r_i and d_x are fixed to 15 nm, 200 nm, 80 nm and 15 nm, respectively. It may be revealed from this figure that the J_{sc} increases with increasing the r_o for TM incidence where maximum J_{sc} of 28.5 mA/cm² is obtained at $r_o = 160$ nm. However, maximum J_{sc} of 27.9 mA/cm² is obtained at $r_o = 180$ for (TE) incidence. At $d_y = d_x = 15$ nm, if the crescent nanohole size is increased, various new modes are excited in the long wavelength region. Additionally, the hole resonances are strengthened with dramatically improved absorption performance as shown in Fig. 3. The filling material through the crescent hole is next studied. Figure 7(a) shows the J_{sc} as a function of the refractive index (n) of the filling material for the TM, TE, and unpolarized incidences. The studied materials are air ($n=1$), SiO₂ ($n=1.45$), Si₃N₄ ($n=1.98$) and SiC ($n=2.6$). Further, the nanohole SiNW has $R=200$ nm, $r_i = 80$ nm, $r_o = 160$ nm, $d_y = 15$ nm, and $d_x = 15$ nm. It is evident that the asymmetrical NW with the air crescent hole has higher light-harvesting performance than the filled nanohole with other materials for all studied polarizations as shown in Fig. 7. Figures 7(b) and 7(c), show the absorption spectra of the NWSCs with air ($n = 1$) and SiO₂ ($n = 1.45$) filled nanoholes. At $n=1$, the high index contrast between the air hole and the silica material with $n=3.5$. Therefore, high field confinement through the active material is obtained with high J of 28.5 (26.5) mA/cm² for TM (TE) polarization. As the filling refractive index increases, the leakage of the field towards the crescent material is increased. Therefore, the J_{sc} is decreased to 25.3 (24.5) mA/cm² at $n=2.6$. If the filling material is set to Si, conventional cylindrical NW with reduced absorption is obtained with J_{sc} of 23.2 (23.4) mA/cm².

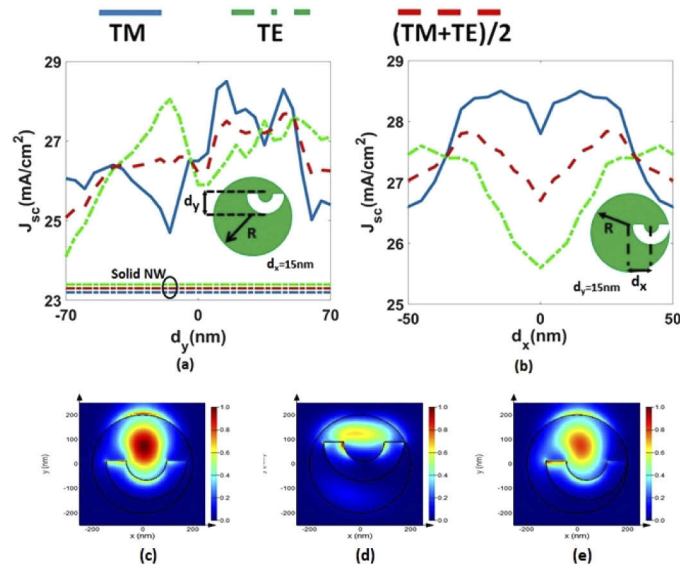


Fig. 7. Short-circuit current density versus (a) the deviance distance d_y at $d_x=15$ nm, and (b) the sidelong deviation d_x at $d_y=15$ nm for TE and TM incidences. The field plot of the norm component of the fundamental TM mode at (c) $d_y=d_x=15$ nm, (d) $d_x=15$ nm and $d_y=70$ nm, and (e) $d_x=40$ nm, and $d_y=15$ nm.

The impact of adding Si substrate and Ag back reflector to the suggested design is also investigated as shown in Fig. 8. In this study, Si substrate of thickness 2000 nm and 200 nm Ag back reflector have been used. It may be seen that an absorption improvement has been obtained for the two polarizations after adding the substrate and Ag back reflector. The proposed SiNW with substrate and back reflector shows higher efficiency of 41.6% and 41.5% than the crescent NW only by 19.5% and 28.08%, for TE and TM polarizations, respectively. This is attributed to the strong coupling between the supported modes by the NW, and that of the underlying substrate [29]. Further, an enhancement of 14.9% and 14.6% has been achieved relative to conventional NW with the same substrate and reflector for the TM and TE polarizations, respectively, as shown in Fig. 8(d).

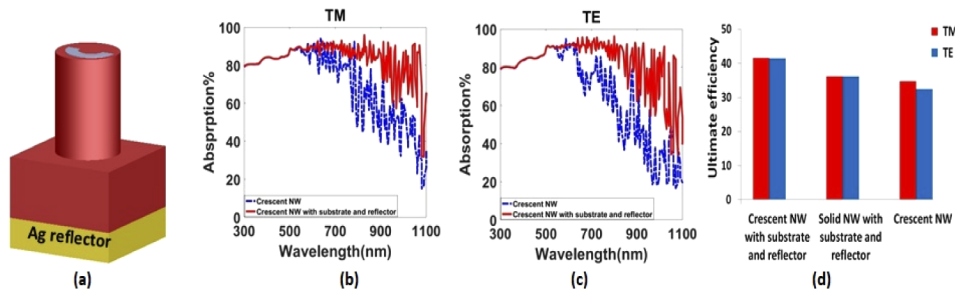


Fig. 8. (a) 3D representation of the reported SiNWs with substrate and back reflector. Variation of the wavelength dependent absorption of the modified NWs for (a) TM and (b) TE polarizations, (d) ultimate efficiency for the crescent NW, solid NW with substrate and back reflector, and proposed crescent NW.

3.2. Electrical results

In this study, the surface recombination velocity between the silicon material and the metal is equal to 10^7 cm/s. In order to have an accurate electrical simulation, the surface recombination velocity, Auger, radiative as well as Shockley–Read–Hall recombination are taken into regard. The total optical generation rate obtained from optical simulation will be imported into the Lumerical Device to solve the drift equation and Poisson equation. In this investigation, the concentration of the p++ type doping is equal to 10^{20} cm⁻³, and that of the p-type doping is 10^{19} cm⁻³, while the n++ type has a concentration of 5×10^{20} cm⁻³. However, the intrinsic i-type doping concentration is equal to 10^{15} cm⁻³ [46]. The electrical parameters used in this study are listed in Table 4.

Table 4. The electrical parameters of the crescent NW SC.

Parameters	Description	Nominal value
μ_p	Hole mobility	470.5 cm ² /V.s
μ_n	Electron mobility	1471 cm ² /V.s
N_D	Donor concentration (n- doping)	10^{17} to 10^{20} cm ⁻³
N_A	Acceptor concentration (p- doping)	1×10^{19} cm ⁻³
n + +		5×10^{20} cm ⁻³
p + +		1×10^{20} cm ⁻³
τ_n	Electron SRH recombination lifetime	3.3μs
τ_p	Hole SRH recombination lifetime	4 μs
C_n , Auger	Auger recombination of electrons for Silicon at 300K	$2.8e^{-31}$ cm ⁶ /s
C_p , Auger	Auger recombination of holes for Silicon at 300K	$9.9e^{-31}$ cm ⁶ /s
$C_{radiative}$	Radiative recombination coefficient for Silicon at 300K	$1.6e^{-14}$ cm ³ /s

Figures 9(a)–9(c) show the current density–voltage (J-V) curves of the reported SiNW with the crescent NH and the conventional solid nanowire counterpart. However, Figs. 9(b)–9(d) illustrate the power density–voltage (P-V curve) under TM and TE incidences. It can be clearly seen from these figures that the proposed NW offers electrical characteristics better than that of the conventional solid NW. The proposed design shows J_{sc} of 33.85 mA/cm², and 34.35 mA/cm², respectively, for the NW with crescent hole under TM (TE) incidences with an enhancement of PCE 16.3 (16.8) % compared to the conventional solid NW. Additionally, the power energy conversion (PCE) of the reported design is 16.78% and 17.05 for TM and TE polarizations, respectively, which is greater than the conventional solid NW by 17.3 (18.4)%. The enhancement in the JV and PV characteristics of the suggested design is basically due to the absorption improvement as shown in Fig. 3(a) and 3(b). Table 5 summarizes the parameters of the electrical performance (V_{oc} , J_{sc} , PCE) of the conventional solid NW and the modified SiNW with crescent hole under TE and TM incidences.

Table 5. Electrical results of the crescent and the solid NW SCs under TE and TM incidences

Parameters	Proposed NW		Solid NW	
	TE	TM	TE	TM
J_{sc} (mA/cm ²)	34.35	33.85	29.4	29.1
V_{oc} (v)	0.61	0.61	0.60	0.60
PCE %	17.05	16.78	14.4	14.3

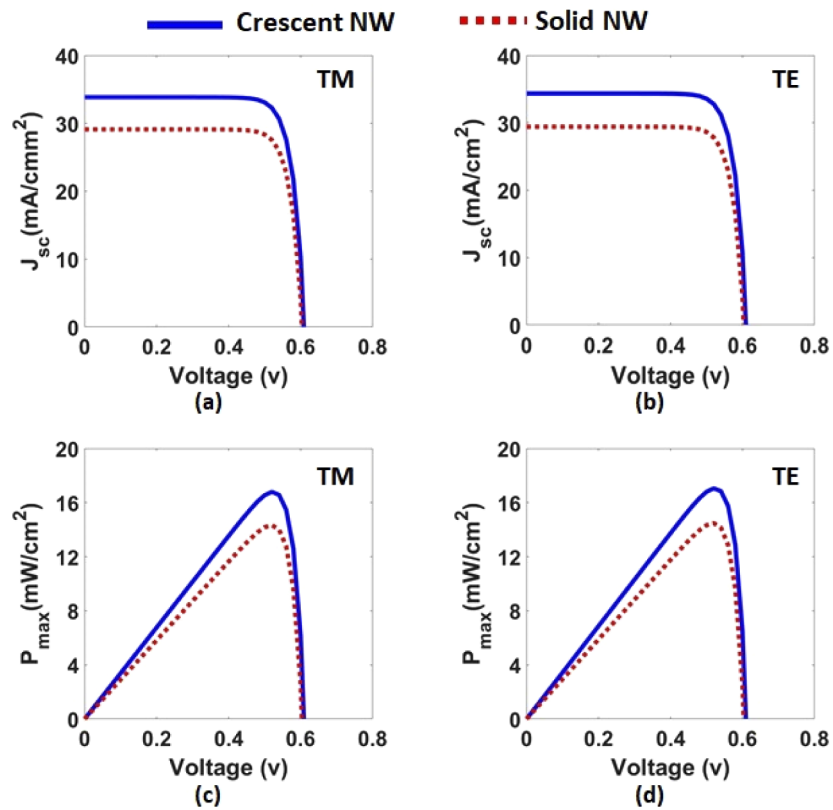


Fig. 9. JV curves of the (a) TM and (b) TE polarized light, and PV curves of the (c) TM and (d) TE polarized light through the crescent NW and solid NW with n-type doping of $3 \times 10^{17} \text{ cm}^{-3}$.

Figures 10(a)–10(b) show the effects of the different doping concentrations on the J_{sc} and the PCE at N_D layer thickness of 250 nm. The N_D concentration is varied from 10^{17} to 10^{20} cm^{-3} while the other concentrations are fixed to their initial values listed in Table 4. It can be seen from this figure that the J_{sc} and PCE are strongly dependent on the N_D value. As N_D increases

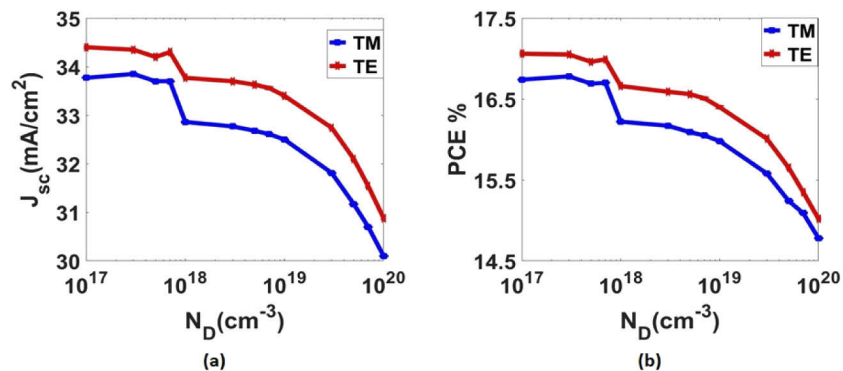


Fig. 10. (a) Variation of the short circuit current density (J_{sc}) and (b) PCE of the crescent NW with n-doping concentration at N_D layer thickness of 250 nm.

from 10^{17} cm to 10^{20} cm $^{-3}$, the J_{sc} decreases from 33.85 (34.4) to 30.1 (30.88) mA/cm 2 and the PCE decreases from 16.78% (17.06%) to 14.78% (15.02%), respectively. The high doping will decrease the carrier lifetime with large carrier recombination losses. Auger recombination, radiative recombination, and Shockley–Read–Hall recombination are responsible for producing these recombination losses. The high doping level decreases dramatically the mobility of the charge-carrier with significant carrier recombination losses [56].

4. Fabrication process

The proposed crescent nanowire SC can be fabricated by a metal assisted chemical etching (MACE) process as reported in [57,58] and shown in Fig. 11. The Si substrate is first cleaned with acetone, ethanol, and deionized water subsequently. The Ag film is then deposited on the Si substrate using thermal evaporation (Fig. 11(a)). Then, the etching process is performed to obtain the cylindrical NW as shown in Fig. 11(b). In order to remove the Ag coating over the nanowire and the Si substrate, a mixed etchant solution of HF and H $_2$ O $_2$ is used with the catalysis (Fig. 11(c)). Next, the crescent NH can be formed using patterned metal disc-in-hole binary (DIHB) arrays as shown in Fig. 11(e). The electron beam lithography, holographic lithography, and reactive ion etching can accurately control the size, shape, and particle spacing with lower inhomogeneity in large arrays. Further, these methods have been previously used for etching crescent shape as reported in [57,58]. Then, the etching process and Ag film removal are made as shown in Figs. 11(e) and 11(f). The final design is illustrated in Fig. 11(g).

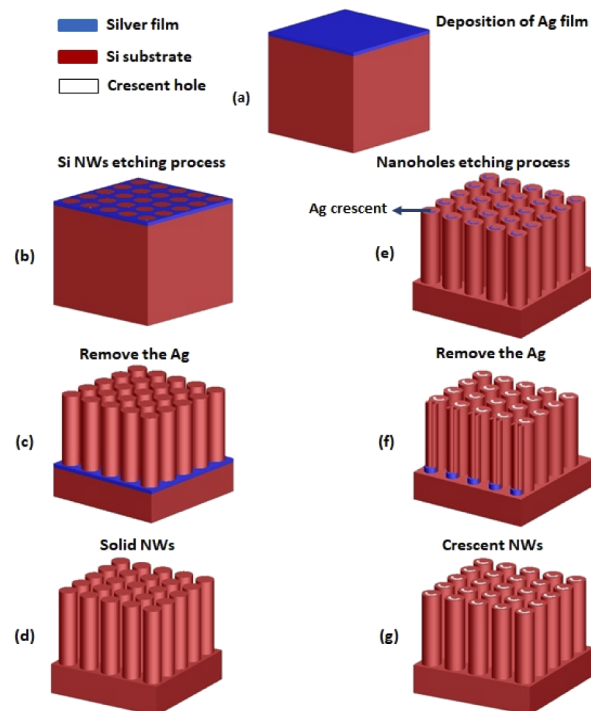


Fig. 11. Flow chart of the fabrication process of the crescent NWSCs using MACE

5. Conclusion

In this paper, a novel design of silicon nanowire with nanocrescent hole is introduced and analyzed. The FEM and FDTD methods are employed to calculate the electrical and optical

characteristics of the reported design. A power conversion efficiency of 16.78 (17.05) % and a short circuit current density of 33.85 (34.35) mA/cm² are achieved with improvement of 17.3 (18.4) and 16.3 (16.8) % compared with the conventional solid cylindrical silicon NW counterpart. This improvement is attributed to the crescent nanohole that can excite highly reinforced optical resonances through the suggested NW.

Funding

Science, Technology and Innovation Funding Authority (STIFA) at Egypt under the Institutional Links Grants. Egypt-UK Cooperation: Newton Mosharafa Program (30732). Grattan acknowledges support from the Royal Academy of Engineering.

Disclosures

The authors declare that there are no conflicts of interest related to this article.

References

1. S. Wang, B. D. Weil, Y. Li, K. X. Wang, E. Garnett, S. Fan, and Y. Cui, "Large-area free-standing ultrathin single-crystal silicon as processable materials," *Nano Lett.* **13**(9), 4393–4398 (2013).
2. S. Jeong, M. D. McGehee, and Y. Cui, "All-back-contact ultra-thin silicon nanocone solar cells with 13.7% power conversion efficiency," *Nat. Commun.* **4**(1), 2950 (2013).
3. K. A. Catchpole and A. Polman, "Plasmonic solar cells," *Opt. Express* **16**(26), 21793–21800 (2008).
4. T. G. Chen, P. Yu, S. W. Chen, F. Y. Chang, B. Y. Huang, Y. C. Cheng, J. C. Hsiao, C. K. Li, and Y. R. Wu, "Characteristics of large-scale nanohole arrays for thin-silicon photovoltaics," *Prog. Photovolt: Res. Appl.* **22**(4), 452–461 (2014).
5. F. Priolo, T. Gregorkiewicz, M. Galli, and T. F. Krauss, "Silicon nanostructures for photonics and photovoltaics," *Nat. Nanotechnol.* **9**(1), 19–32 (2014).
6. C. M. Hsu, S. T. Connor, M. X. Tang, and Y. Cui, "Wafer-scale silicon nanopillars and nanocones by Langmuir–Blodgett assembly and etching," *Appl. Phys. Lett.* **93**(13), 133109 (2008).
7. J. Vukajlovic-Plestina, W. Kim, L. Ghisalberti, G. Varnavides, G. Tütüncüoğlu, H. Potts, M. Friedl, L. Günat, W. Carter, V. Dubrovskii, and A. F. i Morral, "Fundamental aspects to localize self-catalyzed III-V nanowires on silicon," *Nat. Commun.* **10**(1), 869 (2019).
8. M. G. Donato, O. Brzobohatý, S. H. Simpson, A. Irrera, A. A. Leonardi, M. J. Lo Faro, V. Svak, O. M. Maragò, and P. Zemánek, "Optical trapping, optical binding, and rotational dynamics of silicon nanowires in counter-propagating beams," *Nano Lett.* **19**(1), 342–352 (2019).
9. A. M. Gouda, M. Y. Elsayed, A. E. Khalifa, Y. Ismail, and M. A. Swillam, "Random textured silicon oxide nanocones for high-performance thin silicon solar cells," In *Physics, Simulation, and Photonic Engineering of Photovoltaic Devices VII* (Vol. 10527, p. 105270L). International Society for Optics and Photonics (2018, February).
10. L. Saedi, M. Maskanati, M. Modheji, and H. Soleymanabadi, "Tuning the field emission and electronic properties of silicon nanocones by Al and P doping: DFT studies," *J. Mol. Graphics Modell.* **81**, 168–174 (2018).
11. O. Mohsen, A. Lueansaramwong, S. Valluri, V. Korampally, P. Piot, and S. Chattopadhyay, "Field Emission from Silicon Nanocones Cathodes," In *2018 IEEE Advanced Accelerator Concepts Workshop (AAC)* (pp. 1–5). IEEE (2018, August).
12. Y. Ohno and S. Takeda, "Formation process of silicon surface nanoholes," In *Microscopy of Semiconducting Materials 2001* (pp. 395–398). CRC Press (2018).
13. X. Qin, Y. Wu, Z. Xia, J. Zhou, and Z. Zhang, "Beneficial effect of reducing symmetry on the enhancement of optical absorption of nanohole arrays," *Opt. Commun.* **427**, 90–94 (2018).
14. L. Zhao, S. Chen, L. Wang, F. Gao, X. Yao, and W. Yang, "Large-scale fabrication of free-standing and transparent SiC nanohole array with tailored structures," *Ceram. Int.* **44**(6), 7280–7285 (2018).
15. Z. Li, A. Aranda-Ramos, P. Güell-Grau, J. L. Tajada, L. Pou-Macayo, S. L. Piedrafita, F. Pi, A. G. Roca, M. D. Baró, J. Sort, C. Nogués, J. Nogués, and B. Sepúlveda, "Magnetically amplified photothermal therapies and multimodal imaging with magneto-plasmonic nanodomes," *Appl. Mater. Today* **12**, 430–440 (2018).
16. G. Y. Abdel-Latif, M. F. O. Hameed, M. Hussein, M. Abdel Razzak, and S. S. A. Obayya, "Characteristics of highly efficient star-shaped nanowires solar cell," *J. Photonics Energy* **8**(04), 1 (2018).
17. X. Tan, Y. Tu, C. Deng, A. von Czarnowski, W. Yan, M. Ye, and Y. Yi, "Enhancement of light trapping for ultrathin crystalline silicon solar cells," *Opt. Commun.* **426**, 584–588 (2018).
18. H. Shen, N. Asadizanjani, M. Tehranipoor, and D. Forte, "Nanopyramid: An Optical Scrambler Against Backside Probing Attacks," In *ISTFA 2018: Proceedings from the 44th International Symposium for Testing and Failure Analysis* (p. 280). ASM International (2018, December).
19. A. H. K. Mahmoud, M. Hussein, M. F. O. Hameed, M. Abdel-Aziz, H. M. Hosny, and S. S. A. Obayya, "Optoelectronic performance of a modified nanopyramid solar cell," *J. Opt. Soc. Am. B* **36**(2), 357–365 (2019).

20. L. Y. Chen and M. M. Akaisi, "Investigation of Nanopyramids coatings on Perovskite Solar Cell for Performance Enhancement," In *2018 IEEE 7th World Conference on Photovoltaic Energy Conversion (WCPEC)(A Joint Conference of 45th IEEE PVSC, 28th PVSEC & 34th EU PVSEC)* (pp. 0472–0476). IEEE (2018, June).
21. C. Zhen and L. Enling, "Growth and Excellent Field Emission Properties of GaN Nanopencils and Nanotowers," *Rare Metal Mater. Eng.* **47**(1), 43–46 (2018).
22. J. Chen, T. Subramani, W. Jevasuwan, K. Dai, K. Shinotsuka, Y. Hatta, and N. Fukata, "Fabrication of high-performance ordered radial junction silicon nanopencil solar cells by fine-tuning surface carrier recombination and structure morphology," *Nano Energy* **56**, 604–611 (2019).
23. P. Yu, F. Zhang, Z. Li, Z. Zhong, A. Govorov, L. Fu, H. Tan, C. Jagadish, and Z. Wang, "Giant optical pathlength enhancement in plasmonic thin film solar cells using core-shell nanoparticles," *J. Phys. D: Appl. Phys.* **51**(29), 295106 (2018).
24. Y. Park, K. Vandewal, and K. Leo, "Optical In-Coupling in Organic Solar Cells," *Small Methods* **2**(10), 1800123 (2018).
25. O. Höhn, N. Tucher, and B. Bläsi, "Theoretical study of pyramid sizes and scattering effects in silicon photovoltaic module stacks," *Opt. Express* **26**(6), A320–A330 (2018).
26. H. Zhang and J. Toudert, "Optical management for efficiency enhancement in hybrid organic-inorganic lead halide perovskite solar cells," *Sci. Technol. Adv. Mater.* **19**(1), 411–424 (2018).
27. M. N. Esfahani and B. E. Alaca, "Surface Stress Effect on Silicon Nanowire Mechanical Behavior: Size and Orientation Dependence," *Mech. Mater.* **127**, 112–123 (2018).
28. M. Hussein, M. F. O. Hameed, N. F. Areeed, A. Yahia, and S. S. A. Obayya, "Funnel-shaped silicon nanowire for highly efficient light trapping," *Opt. Lett.* **41**(5), 1010–1013 (2016).
29. G. Y. Abdel-Latif, M. F. O. Hameed, M. Hussein, M. A. Razzak, and S. S. Obayya, "Electrical characteristics of funnel-shaped silicon nanowire solar cells," *J. Photonics Energy* **7**(4), 047501 (2017).
30. D. Lee and S. Kim, "Formation of hexagonal Gd disilicide nanowires on Si (100)," *Appl. Phys. Lett.* **82**(16), 2619–2621 (2003).
31. E. Kim, T. Yu, E. Sang Song, and B. Yu, "Chemical vapor deposition-assembled graphene field-effect transistor on hexagonal boron nitride," *Appl. Phys. Lett.* **98**(26), 262103 (2011).
32. F. M. Korany, M. F. O. Hameed, M. Hussein, R. Mubarak, M. I. Eladawy, and S. S. A. Obayya, "Conical structures for highly efficient solar cell applications," *J. Nanophotonics* **12**(01), 1 (2018).
33. G. Niu, G. Capellini, F. Hatami, A. Di Bartolomeo, T. Niermann, E. H. Hussein, M. A. Schubert, H. M. Krause, P. Zaumseil, O. Skibitzki, and G. Lupina, "Selective Epitaxy of InP on Si and Rectification in Graphene/InP/Si Hybrid Structure," *ACS Appl. Mater. Interfaces* **8**(40), 26948–26955 (2016).
34. N. Anttu and H. Q. Xu, "Efficient light management in vertical nanowire arrays for photovoltaics," *Opt. Express* **21**(S3), A558–A575 (2013).
35. C. Colombo, M. Heiß, M. Grätzel, and A. Fontcuberta i Morral, "Gallium arsenide p-i-n radial structures for photovoltaic applications," *Appl. Phys. Lett.* **94**(17), 173108 (2009).
36. P. Krogstrup, H. I. Jørgensen, M. Heiss, O. Demichel, J. V. Holm, M. Aagesen, J. Nygard, and A. F. i Morral, "Single-nanowire solar cells beyond the Shockley–Queisser limit," *Nat. Photonics* **7**(4), 306–310 (2013).
37. S. Geißendörfer, M. Vehse, T. Voss, J. P. Richters, B. Hanke, K. von Maydell, and C. Agert, "Integration of n-doped ZnO nanorod structures as novel light-trapping concept in amorphous thin film silicon solar cells," *Sol. Energy Mater. Sol. Cells* **111**, 153–159 (2013).
38. R. E. Nowak, M. Vehse, O. Sergeev, T. Voss, M. Seyfried, K. von Maydell, and C. Agert, "ZnO Nanorods with Broadband Antireflective Properties for Improved Light Management in Silicon Thin-Film Solar Cells," *Adv. Opt. Mater.* **2**(1), 94–99 (2014).
39. B. Tian, X. Zheng, T. J. Kempa, Y. Fang, N. Yu, G. Yu, J. L. Huang, and C. M. Lieber, "Coaxial silicon nanowires as solar cells and nanoelectronic power sources," *Nature* **449**(7164), 885–889 (2007).
40. T. Stelzner, M. Pietsch, G. Andrä, F. Falk, E. Ose, and S. Christiansen, "Silicon nanowire-based solar cells," *Nanotechnology* **19**(29), 295203 (2008).
41. G. Jia, M. Steglich, I. Sill, and F. Falk, "Core-shell heterojunction solar cells on silicon nanowire arrays," *Sol. Energy Mater. Sol. Cells* **96**, 226–230 (2012).
42. K. Q. Peng and S. T. Lee, "Silicon nanowires for photovoltaic solar energy conversion," *Adv. Mater.* **23**(2), 198–215 (2011).
43. J. Zhu, Z. Yu, G. F. Burkhard, C. M. Hsu, S. T. Connor, Y. Xu, Q. Wang, M. McGehee, S. Fan, and Y. Cui, "Optical absorption enhancement in amorphous silicon nanowire and nanocone arrays," *Nano Lett.* **9**(1), 279–282 (2009).
44. J. Cho, B. O'Donnell, L. Yu, K. H. Kim, I. Ngo, and P. R. I. Cabarrocas, "Sn-catalyzed silicon nanowire solar cells with 4.9% efficiency grown on glass," *Prog. Photovolt: Res. Appl.* **21**(1), 77–81 (2013).
45. L. W. Veldhuizen, Y. Kuang, and R. E. I. Schropp, "Ultrathin tandem solar cells on nanorod morphology with 35-nm thick hydrogenated amorphous silicon germanium bottom cell absorber layer," *Sol. Energy Mater. Sol. Cells* **158**, 209–213 (2016).
46. Z. Yang, X. Li, D. Y. Lei, A. Shang, and S. Wu, "Omnidirectional absorption enhancement of symmetry-broken crescent-deformed single-nanowire photovoltaic cells," *Nano Energy* **13**, 9–17 (2015).
47. M. L. Brongersma, Y. Cui, and S. Fan, "Light management for photovoltaics using high-index nanostructures," *Nat. Mater.* **13**(5), 451–460 (2014).

48. Z. Xia, X. Qin, Y. Wu, Y. Pan, J. Zhou, and Z. Zhang, "Efficient broadband light absorption in elliptical nanohole arrays for photovoltaic application," *Opt. Lett.* **40**(24), 5814–5817 (2015).
49. C. Zhang, Z. Yang, K. Wu, and X. Li, "Design of asymmetric nanovoid resonator for silicon-based single-nanowire solar absorbers," *Nano Energy* **27**, 611–618 (2016).
50. <https://www.lumerical.com/>
51. E.D. Palik, *Handbook of Optical Constants of Solids*, (Academic Press, Orlando, 1985).
52. W. M. Robertson, G. Arjavalingam, R. D. Meade, K. D. Brommer, A. M. Rappe, and J. D. Joannopoulos, "Measurement of photonic band structure in a two-dimensional periodic dielectric array," *Phys. Rev. Lett.* **68**(13), 2023–2026 (1992).
53. O. Kilic, M. Dignonnet, G. Kino, and O. Solgaard, "Controlling uncoupled resonances in photonic crystals through breaking the mirror symmetry," *Opt. Express* **16**(17), 13090–13103 (2008).
54. G. Gomard, R. Peretti, S. Callard, X. Meng, R. Artinyan, T. Deschamps, P. R. i Cabarrocas, E. Drouard, and C. Seassal, "Blue light absorption enhancement based on vertically channelling modes in nano-holes arrays," *Appl. Phys. Lett.* **104**(5), 051119 (2014).
55. C. Zhang, Z. Yang, A. Shang, S. Wu, Y. Zhan, and X. Li, "Improved optical absorption of silicon single-nanowire solar cells by off-axial core/shell design," *Nano Energy* **17**, 233–240 (2015).
56. M. A. Green, *Solar Cells: Operating Principles, Technology, and System Applications*, (Prentice Hall Inc., Englewood Cliffs, New Jersey, 1982).
57. A. K. Sheridan, A. W. Clark, A. Glidle, J. M. Cooper, and D. R. S. Cumming, "Multiple plasmon resonances from gold nanostructures," *Appl. Phys. Lett.* **90**(14), 143105 (2007).
58. R. Liu, F. Zhang, C. Con, B. Cui, and B. Sun, "Lithography-Free Fabrication of Silicon Nanowire and Nanohole Arrays by Metal-Assisted Chemical Etching," *Nanoscale Res. Lett.* **8**(1), 155 (2013).